

# Photon flux characterization of a new electron LINAC in the CINPHONIE irradiation facility

Benoit Geslot\*, Nicolas Estre, Emmanuel Payan, Daniel Eck, Frédéric Moutet, Alix Sardet, Malo Lebreton, Cédric Carasco, Bertrand Perot  
CEA, DES, IRESNE, DTN, SMTA, Nuclear Measurement Laboratory, Cadarache, F-13108 St Paul  
Lez Durance, France  
(\* ) corresponding author: [benoit.geslot@cea.fr](mailto:benoit.geslot@cea.fr)

**Abstract**— Electron linear accelerators (LINACs) are versatile and powerful X-ray sources, that can be used in medical radiotherapy as well as in various industrial applications including non-destructive testing, imaging and security inspection. LINACs accelerate electrons by passing them through a series of oscillating electric fields within a vacuum tube. These high-energy electrons are then directed towards a metallic target, producing X-rays (bremsstrahlung radiation) when they decelerate upon impact. In the field of non-destructive radioactive waste characterization, high-energy photon imaging (radiography, tomography) is used on large cemented radiological waste containers, with a volume of the order of  $1\text{ m}^3$ , to check their integrity and assess their content [1][2]. However, for such packages, passive gamma-ray spectroscopy, passive neutron counting and even active neutron interrogation fail in measuring nuclear materials, like plutonium and uranium. Therefore, high-energy photon interrogation techniques is under study to detect and quantify nuclear materials through the detection of induced-photofission particles. For the past years, CEA has been developing high-energy imaging [3] and photon interrogation techniques in CINPHONIE irradiation bunker (CHICADE facility, CEA IRESNE, Cadarache, France). CINPHONIE was recently upgraded with a K15 Varex accelerator that can reach a maximum dose rate of 130 Gy/min at 1 m from the X-ray target [4]. For advanced techniques (high-energy photon and photoneutron activations, photofission, bi-energy imaging), it is paramount to simulate precisely the irradiation field. For that purpose, a numerical model of the LINAC internals was built (with MCNP 6.3). It aims at simulating photon and neutron fields in view to calculate dose rates and reaction rates in irradiation samples, waste packages, but also in the whole casemate. A thorough characterization campaign was carried out to validate and calibrate this MCNP model against various experiments, including dose rate measurements in a water tank and delayed gamma-ray spectroscopy of thin metal foils activated in the X-ray field. These experimental results were used to fine-tune the electron source energy distribution as well as to estimate the average beam current. Its high-energy part is indeed particularly crucial for photofission and bi-energy studies.

**Keywords** —Photo-activation, Active photon interrogation, LINAC, Bremsstrahlung, CINPHONIE

## I. INTRODUCTION

THE Nuclear Measurement Laboratory (CEA Cadarache) has long been developing non-destructive measurements in the context of inspection and characterization of nuclear waste packages [1], such as passive gamma spectrometry (global or segmented), passive neutron counting, high energy imaging (radiography, tomography), active neutron interrogation (prompt or delayed neutron measurement) or active photon interrogation [5].

The CINPHONIE irradiation bunker, located in the CHICADE facility (Cadarache, France) is dedicated to inspecting large and dense objects, such as 870 L cemented waste drums. Coupled to a motorized 3-axis bench, objects of dimensions up to 1.6 m in diameter and 5000 kg in mass can be handled. CINPHONIE was recently equipped with a new high energy X-ray source: a Varex K15 LINAC [2]. The LINAC was installed and commissioned in June 2024. The stability of the dose rate, as well as the reproducibility of irradiation conditions have been greatly improved compared to previous setups with a legacy SATURNE LINAC [4].

The K15 can be operated in two irradiation modes. In the so-called “high energy mode”, the maximum dose rate reaches 130 Gy/min (at 1 m from the Bremsstrahlung target). In this mode, the photons have sufficient energy to induce activation by  $(\gamma, xn)$  reactions on the surrounding materials. In the “low dose rate” mode, the beam energy is lowered (around 9 MeV) so as to drastically reduce photo-activation. The maximum dose rate in this mode is 23 Gy/min @ 1 m.

To correctly predict dose rates (gamma and neutron), material activation and reaction rates of interest, such as photofission in nuclear material, Monte Carlo simulations with MCNP 6.3 are extensively used. A realistic model based on the geometry and materials of the LINAC interns (Bremsstrahlung target, collimator and shielding) was built and used to simulate the X-ray field (spectrum and geometry). This article is focused on the experiments that were carried out to validate and calibrate the MCNP model.

One of the main parameters of the simulations is the source definition and more specifically the average electrons' energy. Varying the electron energy or, to a minor extent, the distribution of energy can drastically change the results. In order to compare simulation results to experiments, the beam current needs also to be estimated.

## II. DESCRIPTION OF THE EXPERIMENTS

### A. Experimental setup

Calibration tests were carried out with the objective of estimating the electron average beam's energy and current. First, the total dose rate deposited in a water tank was measured using an ionizing chamber (PTW equipped an electrometer). By fitting the attenuation curves along the beam's axis, it was possible to estimate the linear attenuation coefficient and to compare it to simulation results at various beam's energies. This was done in both operating modes.

Complementarily, photo-activation experiments were carried out with the objective to obtain more information on the high energy part of the X ray field. Photo-activation reactions like  $(\gamma, xn)$  are only possible when the photon's energy is above the minimum binding energy of nucleons (typically a few MeV). When reaching this threshold, the nucleus enters the Giant Dipole Resonance (GDR), which may result in the emission of neutrons and gamma rays.

By irradiating metal foils of gold, nickel and depleted uranium, short-lived radionuclides were produced by  $(\gamma, n)$  and  $(\gamma, f)$  reactions and then measured on a gamma spectrometry bench equipped with an hyper pure germanium detector and a Canberra acquisition system with Genie-2000 software. Interestingly, the four reactions of interest have different energy thresholds (see table I). This explains why their sensitivity to the beam's energy vary greatly.

TABLE I  
REACTIONS OF INTEREST FOR PHOTO-ACTIVATION EXPERIMENTS, ENERGIES AND INTENSITIES OF GAMMA RAYS (SOURCE: LNH)

Reaction	Threshold (MeV)	Radionuclide	Half-life	Energy (keV)	Intensity (%)
$^{197}\text{Au}(g,n)$	8.5	$^{196}\text{Au}$	6.18 d	333 355	22.9 87
$^{58}\text{Ni}(g,n)$	12	$^{57}\text{Ni}$	1.5 d	127 1377	16 81.2
$^{238}\text{U}(g,n)$	6.5	$^{237}\text{U}$	6.75 d	208	21.3
$^{238}\text{U}(g,F)$	5	$^{135}\text{I}$	6.57 h	1131 1260	22.6 28.7
$^{238}\text{U}(g,F)$	5	$^{92}\text{Sr}$	2.65 h	1384	90

The metal foils were mounted on a 3D-printed plastic holder, the center of which was aligned with respect to the beam's axis (X axis). The measurement's reference point was located at 104.4 cm from the X-ray target (referred to as "position 1"). It corresponds to the aluminum door mounted on the K15 collimation system. This door was customized with a central housing to accommodate the plastic holder. Several irradiations were performed in position 1 to check the reproducibility and consistency in the results.

A second configuration located further away from the target (X = 242 cm, referred to as "position 2") was explored with the objective of mapping the gold and nickel reaction rates on a square grid with a pitch of 3 cm.

Prior to the irradiations, the metal foils were weighted to account for small variations in their mass. Then they were put in small 3D-printed "pill box" loaded with 3 nickel disks (each 1 mm in thickness, ~1.55 g) on top of which a thin gold foils was taped (0.1 mm in thickness, ~95 mg).

After irradiation, each set of disks was measured altogether, putting the gold foils on the bottom side, the closest to the HPGC diode.

The metallic uranium 238 disk (0.1 mm in thickness, ~100 mg) was irradiated and measured separately, in a vinyl bag for radioprotection. The bag was taped on the plastic holder, so as to center the uranium disk with respect to the X axis.

In both setups, the metal foils were arranged symmetrically with respect to the beam axis (X axis), either diagonally or vertically (or in both directions in the case of configuration #6, see table II). Symmetrical positions were chosen to check the alignment of the beam with the X axis.

TABLE II  
LIST OF IRRADIATION CONFIGURATIONS

	Dura-tion	Position	Number of disks (gold, nickel, U)	Setup	Average dose rate (Gy/min)*
#1	1 h	1	1 - 1 - 0	Central	127.9
#2	1 h	1	3 - 3 - 0	Diagonal	126.1
#3	1 h	1	3 - 3 - 0	Diagonal	129.3
#4	1 h	1	0 - 0 - 1	Central	131.5
#5	1 h	1	3 - 3 - 0	Vertical	131.0
#6	2 h	2	10 - 10 - 0	Diagonal & Vertical	132.4

\* The dose rate and dose were recorded by the LINAC's monitoring system.

### B. Monte Carlo simulations

The MCNP 6.3 particle transport code, associated with the IAEA PD-2019 photo-nuclear cross sections library, was used to calculate photon spectra (illustration on Fig. 1, left) and photo-activation reaction rates inside the metal disks (using F4 tallies with flux modifiers FM card).

After analyzing configurations #2 and #3, a small shift of the position of the maximum flux was discovered. To account for this bias in the simulation, the beam axis was shifted by +5 mm vertically at X = 104 cm and by +12 mm at X = 242 cm (illustration on Fig. 1, right).

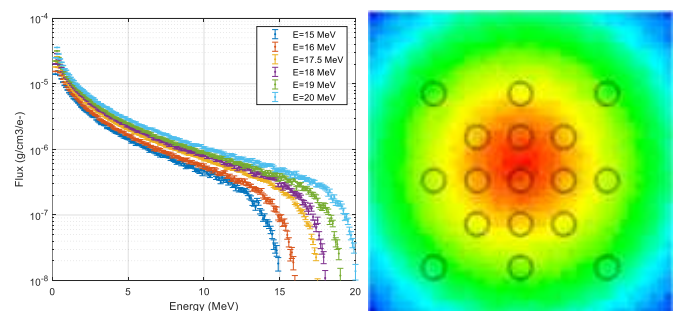


Fig. 1: Photon spectra for various energy of the beam (left). Flux mesh in the Y-Z plane for configuration #6 (right): the black circles represent the activation foils containers.

## III. RESULTS AND DISCUSSION

### A. Total dose rate in water

The photon dose rate deposited in water is sensitive to the whole photon spectrum, which is mainly composed of photons below 5 MeV. MCNP F6 tallies were used to calculate the total dose rate in the water tank. The volume of cells was chosen

equal to the sensitive volume of the ionization chamber.

By varying the beam's energy, several attenuation curves were produced. They are displayed on Fig. 2, along with the measurement data points (square markers). All curves show the same behavior: a short increase followed by a typical exponential decay. By dividing measurements dose rates with the beam current (108  $\mu\text{A}$ , estimated based on information issued by the monitoring system), it was possible to directly compare simulations and experiments. It appears that they fall in between simulations obtained with 17.5 MeV and 18 MeV for the beam's energy.

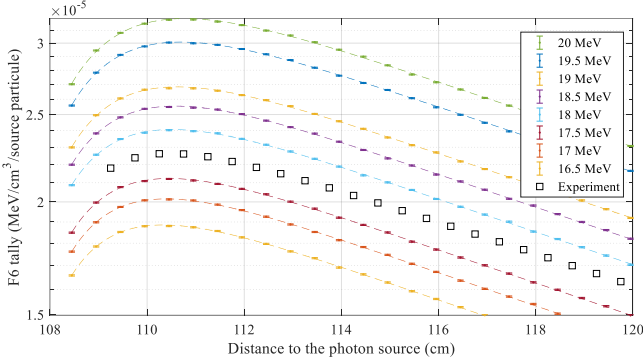


Fig. 2. Dose rate vs. distance in water calculated with MCNP (F6 tally) and measurement (scaling factor with a beam current of 108  $\mu\text{A}$ )

### B. Photo-activation results

After the irradiation, the metal foils were placed on the gamma spectrometry bench for counting. Then, the analysis process was as follows: counting spectra were processed to obtain integral counts in the photopeaks of interest (see table I). Knowing the detector's efficiency  $\varepsilon$  (based on an MCNP 6.3 model), the decay constant  $\lambda$  of the radionuclide, the intensity of gamma rays  $I_\gamma$  and the mass of the metal disk  $M$ , the measurement  $C$  could be converted into an activity per mass unit  $A$  (in Bq/g), as expressed in equation (1).

$$A = \frac{\lambda}{M \varepsilon I_\gamma} \frac{1}{(1 - e^{-\lambda T_i}) \cdot e^{-\lambda T_c} \cdot (1 - e^{-\lambda T_m})} C \quad (1)$$

In the previous equation,  $T_i$ ,  $T_c$  and  $T_m$  are the durations of the irradiation, cooling down and measurement phase. By dividing  $A$  by electronic charge  $q_e$  and by the reaction rate simulated with MCNP, an estimation of the average beam's current  $I_X$  can be obtained. In equation (2), the MCNP tally for reaction X is referred to as  $RR_X$  and expressed in  $\text{s}^{-1}/\text{g}/\text{source}$  particle.

$$I_X(E) = \frac{1}{q_e} \frac{A}{RR_X(E)} \quad (2)$$

$RR_X$  strongly depends on the beam's energy  $E$ . By varying  $E$  from 16 MeV to 20 MeV, a list of beam's currents was obtained. All curves should cross at the LINAC operating point that best reflects the measurements. Results displayed on Fig. 3 were produced based on the measurements obtained in configurations #1 and #4. As expected, the curve associated with the  $^{58}\text{Ni}(\gamma, n)$  reaction is the most sensitive to the beam's energy, since the threshold of the reaction is the highest (12 MeV). On the contrary, the reaction  $^{238}\text{U}(\gamma, n)$  gives the flattest curve.

The four reactions give consistent estimations of the average for a beam's energy sitting between 18 MeV and 18.2 MeV. This is in good agreement with the estimation obtained from the dose rate measurements.

Uncertainties associated with the gamma spectrometry measurements are so low (below 1 %) that they cannot be seen on the graph, but there are other sources, as listed below:

- LINAC's reproducibility (around 2 %);
- Efficiency of the detector (typically around 5 %);
- Geometry errors associated to the irradiation setup (position of the metal foils and distance to the X-ray source);
- Geometry errors during gamma spectrometry measurements;
- Photo-nuclear cross sections (around 10 % to 15 %).

The uncertainty breakthrough is clearly dominated by the photo-nuclear cross sections. Under the assumption that the four cross sections are independent from each-others, it is hopefully possible to benefit from the average of the four estimations.

A best estimate of the beam's current was obtained by averaging of the 8 data points lying between 18 MeV and 18.2 MeV. The associated uncertainty was obtained based on the data point experimental standard deviation (square box in Fig. 3). The beam current was estimated at  $(94 \pm 5) \mu\text{A}$ .

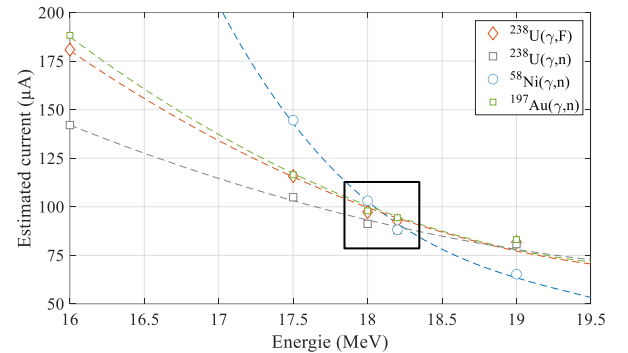


Fig. 3. Average beam's current obtained from activities and analyzed with various beam's energy simulations. Polynomial fit curves are illustrative.

### IV. CONCLUSIONS AND OUTLOOKS

A new X-ray source was installed in the CINPHONIE irradiation casemate and commissioned in 2024. Improved irradiation conditions, in terms of dose rate and reproducibility, are expected from this upgrade.

An MCNP 6.3 model was built and validated against experiments. Dose rate attenuation in water and photo-activation of metal foils were carried out. This article focused on the photoactivation results. Thanks to four reactions of interest, it was possible to estimate two key parameters: the electron beam's average energy and the beam's current. The uncertainty breakdown is dominated by the uncertainties on photo-nuclear cross sections. The beam's energy was estimated at  $(18.1 \pm 0.1) \text{ MeV}$ . The best estimate of the beam's current was  $(94 \pm 5) \mu\text{A}$ .

In future works, a methodology based on Bayesian inference will be used to extract more information from the photo-activation measurements. Indeed, two sets of experimental data

were produced (for the irradiation setups) and they should be analyzed altogether within an enlarged mathematical model. This model will allow estimating extra parameters, such as the distance to the X-ray source and the position of the maximum of the X-ray field. Thanks to the Bayesian framework, uncertainties, especially those associated to the photo-activation cross sections, will be natively included into the estimation process.

#### REFERENCES

- [1] B. Pérot, *et al.*, “The characterization of radioactive waste: a critical review of techniques implemented or under development at CEA, France,” *EPJ Nuclear Sciences & Technologies*, 4, 3 (2018).  
[doi.org/10.1051/epjn/2017033](https://doi.org/10.1051/epjn/2017033)
- [2] N. Estre, *et al.*, “Performances of 9 to 15 MV Computed Tomography of large objects in industrial or nuclear field,” 10<sup>th</sup> International Symposium on Digital Industrial Radiography and Computed Tomography (DIR 2025), Paris, 1-3 July 2025
- [3] M. Kistler, *et al.*, “Simulated performances of very high energy detectors for non-destructive computed tomography characterization of large objects,” *IEEE Transactions on Nuclear Science*, 65(9):2527–2532, 2018.
- [4] N. Estre, *et al.*, “High-Energy X-Ray Imaging Applied to Nondestructive Characterization of Large Nuclear Waste Drums,” *IEEE Transactions on Nuclear Science*, 62(6), 3104–3109, (2015).  
[doi.org/10.1109/TNS.2015.2498190](https://doi.org/10.1109/TNS.2015.2498190)
- [5] M. Delarue, *et al.*, “New measurements of cumulative photofission yields of <sup>239</sup>Pu, <sup>235</sup>U and <sup>238</sup>U with a 17.5 MeV Bremsstrahlung photon beam and progress toward actinide differentiation,” *Nuclear Instruments and Methods in Physics Research Section A: Accelerators, Spectrometers, Detectors and Associated Equipment*, 1040, 167259, (2022).  
[doi.org/10.1016/J.NIMA.2022.167259](https://doi.org/10.1016/J.NIMA.2022.167259)